

Archive ouverte UNIGE

https://archive-ouverte.unige.ch

Article scientifique

Article

2010

Accepted version

Open Access

This is an author manuscript post-peer-reviewing (accepted version) of the original publication. The layout of the published version may differ .

Supramolecular n/p-heterojunction photosystems with oriented multicolored antiparallel redox gradients (OMARG-SHJs)

Bhosale, Rajesh; Misek, Jiri; Sakai, Naomi; Matile, Stefan

How to cite

BHOSALE, Rajesh et al. Supramolecular n/p-heterojunction photosystems with oriented multicolored antiparallel redox gradients (OMARG-SHJs). In: Chemical Society reviews, 2010, vol. 39, n° 1, p. 138–149. doi: 10.1039/b906115k

This publication URL: https://archive-ouverte.unige.ch/unige:4866

Publication DOI: 10.1039/b906115k

© The author(s). This work is licensed under a Other Open Access license https://www.unige.ch/biblio/aou/fr/guide/info/references/licences/

Supramolecular n/p-heterojunction photosystems with oriented multicolored antiparallel redox gradients (OMARG-SHJs)

Rajesh Bhosale, Jiri Misek, Naomi Sakai* and Stefan Matile*

.

Directional electron and hole transport along sophisticated redox gradients to and from the active site are essential in photosynthesis. In the comparably simple bilayer organic solar cells, electron and hole transport occurs in adjacent bulk layers of *n*- and *p*-semiconductors after exciton dissociation at the interface. Maximized exciton dissociation at the maximized interfaces in *n*/*p*-heterojunction (BHJ) solar cells comes at the cost of reduced hole and electron mobility in less continuous donor and acceptor domains. Increasing organization of BHJs ultimately leads to the situation where *n*- and *p*-semiconductors are separated and aligned next to each other continuously on the molecular level, that is supramolecular *n*/*p*-heterojunctions (SHJs). In the bioinspired ideal, electrons and holes would be generated and rapidly carried away in opposite directions by oriented multicolored antiparallel redox gradients (OMARGs) in the adjacent *n*- and *p*-channels of SHJs. In this *tutorial review*, we outline the concept of OMARG-SHJs and summarize recent progress with new approaches to get there. This conceptually innovative twist distilled from an interdisciplinary, timely and very busy topic should appeal to the synthetic organic, supramolecular, biological, physical, analytical and materials chemist as well as to the expert in energy and environmental sciences.

20 1 Introduction

In biological photosystems, excitation of the special pair of chlorophylls (a₁, Figure 1a) is followed by directional, ultrafast electron transfer cascade along sophisticated redox gradients to the remote ubiquinone acceptor (a₆, Figure 1a).^{1,2}
The hole left behind is transferred in the other direction along an orthogonal redox gradient to ultimately oxidize water. These cascade electron / hole transfer pathways are essential for the efficiency of photosynthesis, and held together in antiparallel manner by a large protein embedded in the bilayer membrane.

In organic solar cells, a macroscopic layer of electron- or nsemiconducting material is placed next to a hole- or psemiconducting layer. In such a bilayer configuration,³ photogenerated excitons dissociate at the donor-acceptor 35 interface into electrons and holes that move to their respective final destination and generate photocurrent. Increases of active interface by blending the two conductors resulted in dramatically increased efficiencies of photosystems. Reminiscent of the maximized surface area of thylakoid 40 membranes in chloroplasts, the interlaced donor/acceptorlayers in organic solar cells are usually referred to as bulk n/pheterojunctions (BHJs) (Figure 1b).4 Maximized exciton dissociation achieved at maximized interfaces in BHJ solar cells comes at the cost of reduced hole and electron mobility 45 in poorly organized, increasingly discontinuous donor and acceptor domains. Top-down approaches to improve the organization, and thus the conductivity include the use of differential solubilizers, dendritic polymers, covalent dyad systems, mixed crystals, and so on.4-9 50 organization of BHJs ultimately leads to the situation where

n- and p-semiconductors are separated and aligned on the molecular level, that is supramolecular n/p-heterojunctions (SHJs) (Figure 1c). The bottom-up nature of this approach allows for the rational design of ordered nanostructures not so only to achieve high conductivity but also to implement complexity in the system. However, lessons from nature call for much more, namely SHJ architectures that come in colors everywhere to capture as much light as possible and quickly funnel electrons and holes in opposite directions to the electrodes along oriented co-axial molecular n- and p-semiconductor channels. In the following, this bioinspired ideal SHJ architecture is called OMARG-SHJ, that is an SHJ with oriented multicolored antiparallel redox gradients (Figure 1d).

The creation of OMARG-SHJs is far from possible today because of the exceptional challenges involved. progress made toward OMARG-SHJs is summarized in this review. Before focusing on surface architectures, we briefly summarized methods of characterization and highlight 70 pioneering approaches toward SHJs in solution. discussion of oriented SHJs on surfaces begins with selected examples for the "fuzzy" architectures obtained from layerby-layer (LBL) assembly. From there, we zoom in on recent pioneering approaches to reorient LBL-architectures in 75 polymer brushes or to install interdigitating inter- and intralayer recognition motifs in LBL architectures to build oriented SHJs on solid grounds. The following chapter on photosystems with redox gradients discusses first covalent approaches with self-assembled monolayers SAMs, including 80 examples for the usefulness of biological scaffolds such as DNA duplexes or α-helices to address specific topics. From there, pioneering breakthroughs with 3D architectures with gradients are summarized, oriented redox increasingly organized LBL systems and coordinative 85 covalent capture approaches. After a brief summary of

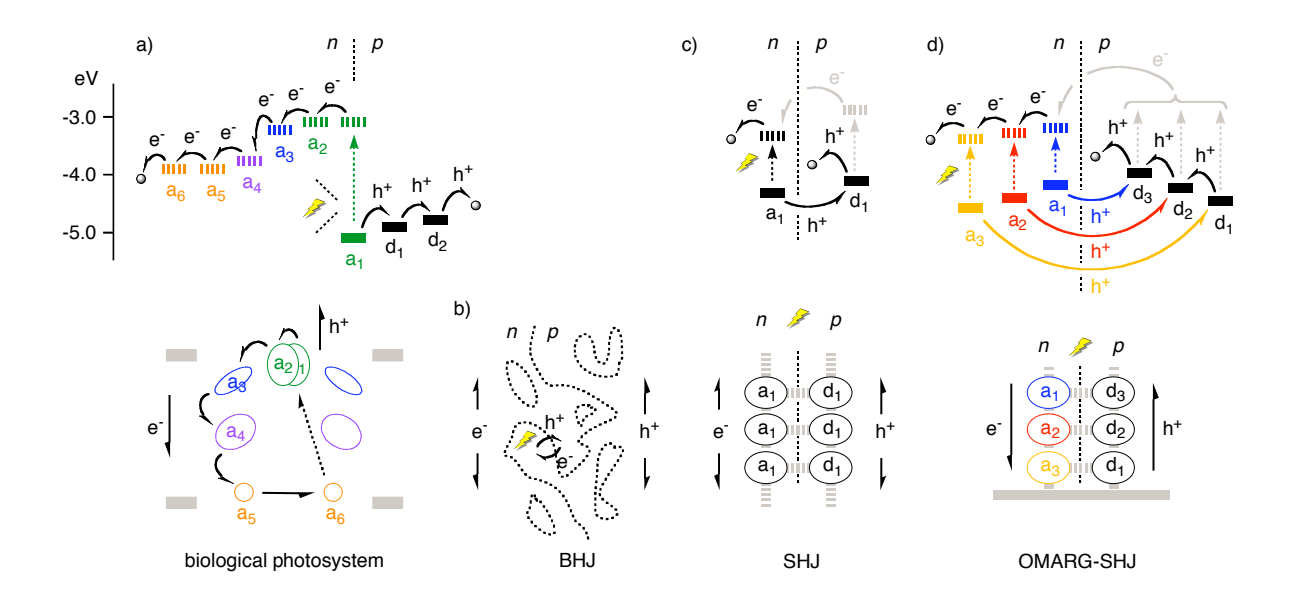


Fig. 1 Energetics (top; solid, HOMO; dashed, LUMO) and architectures (bottom) of electron (e⁻; a, electron acceptors) and hole (h⁺; d, electron donors = hole acceptors) transfer cascades to the final destinations (e.g., electrodes; grey circles in a, d) in (a) biological photosystems (a_1/a_2 , chlorophyll special pair; a_3/a_6 , ubiquinone), (b) BHJs in organic solar cells, (c) SHJs, and (d) OMARG-SHJs. In OMARG-SHJs, excitation of acceptors a_n of different color can be followed by donor-acceptor n/p-charge separation and electron and hole transfer down antiparallel redox gradients toward their final destination; donor excitation followed by electron (rather than energy) transfer to acceptors a_n (grey) leads to the same situation and is thus additive.

rainbow systems, we combine all separate topics to close with emerging approaches toward OMARG-SHJs.

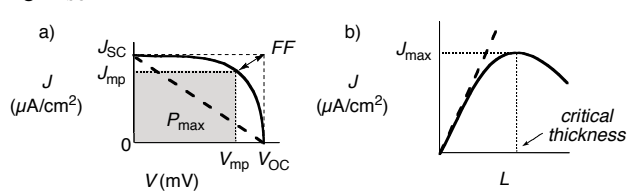
2 Characterization methods

The characterization of synthetic supramolecular photosystems covers many different aspects. Essential insights come from the determination of HOMO-LUMO levels by cyclic voltammetry and absorption spectroscopy, ultrafast photophysics to characterize charge separation (CS) and charge recombination (CR) kinetics or structural studies with various spectroscopic, microscopic, crystallographic and acoustic methods. However, the heart of the matter are *J-V* and *J-L* curves, plots or profiles: They reveal the essential characteristics of the functional system by direct functional feedback (Figure 2).

100 J-V curves describe the dependence of the photocurrent density (J) on the applied voltage (V). Key parameters in J-V curves include the short circuit current density J_{SC} , the open circuit voltage V_{OC} , and most importantly, maximal output power P_{max} (the grey area in Figure 2a) with the 105 corresponding J_{mp} and V_{mp} . The fill factor $FF = J_{\text{mp}} \times V_{\text{mp}} / J_{SC} \times V_{OC}$ describes the squareness of the J-V curve, and is a commonly used parameter to describe P_{max} (= $FF \times J_{SC} \times V_{OC}$). Linear ("ohmic") J-V curves have a low $FF_{\text{min}} = 0.25$. Optimized BHJ solar cells have $FF_{\text{BHJ}} \sim 0.61$. The power 110 conversion efficiency is defined as $\eta_{\text{eff}} = P_{\text{max}} / P_{\text{in}} \times 100\%$ where P_{in} is the irradiance. Leading BHJ solar cells have $\eta_{\text{eff}} \sim 5\%$.

With the increasing organization of n- and psemiconducting pathways, 11 OMARG-SHJs are expected to
have high FF. At high FF, $V_{\rm OC}$ is determined by the energy difference between HOMO of donor and LUMO of acceptor and strongly influenced by other parameters such as device

connection in series. OMARG-SHJs could have high $V_{\rm OC}$ because it is presumably not the smallest but either the proximal or perhaps even the maximal HOMO-LUMO difference in a redox gradient that matters. Because they collect much light, OMARG-SHJs should have comparably high $J_{\rm SC}$.



125 **Fig. 2** "Ohmic" (dashed) and "non-ohmic" (solid) J-V curve (a) and linear (dashed) and bell-shaped (solid) J-L curves (b) with indication of key parameters. Ideal OMARG-SHJs should have non-ohmic J-V with high J_{SC} , V_{OC} and FF as well as linear J-L with unsaturable J_{max} and critical thickness.

density on the layer thickness or number of layers deposited on the surface. In general, the higher the absorbance of the layer, the more charges are generated and thus, the higher *J.* Therefore, at the beginning, *J-L* curves are usually linear (Figure 2b). At a critical thickness, *J-L* curves can saturate at *J*_{max} and flatten out or even decrease with increasing thickness (Figure 2b, bold). If evidence for continuing growth after the photocurrent saturation is secured, then the critical thickness is of highest interest because it indicates the distance holes and electrons can travel without meeting each other to recombine. In OMARG-SHJs, the generated charges should be immediately driven away from each other, and thus very large critical thickness could be expected.

Important information beyond *J-V* and *J-L* curves comes from action spectra, quantifying the photocurrents generated by individual chromophores, and AFM images, describing the

surface roughness of the artificial photosystems (smooth surfaces have been associated with highly ordered structures and thus high efficiencies).⁶

Comparison of different systems has to be done with caution, as different conditions can in general affect the outcome with supramolecular functional systems dramatically.

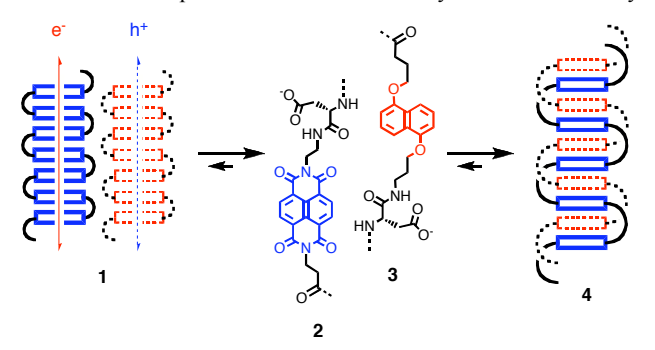


Fig. 3 Programmed assembly of π -acidic and π -basic oligomers 2 and 3 into charge-transfer duplex 4 rather that the notional SHJ architecture 1.

3 SHJs

Common aromatics (e.g., benzenes) are π -basic and characterized by a negative quadrupole moment (e.g., $Q_{zz} = -8.5\,$ B). Their electron-rich surfaces allow cation- π interactions and formation of p-semiconducting π -stacks (e.g., hexabenzocoronenes, HBCs). The much more exotic π -acidic aromatics (e.g., hexafluorobenzene) have a positive quadrupole moment (e.g., $Q_{zz} = +9.5\,$ B) and an electron-poor surface to attract anions, and their π -stacks can be n-165 semiconductors (e.g., naphthalenediimides, NDIs). SHJs are a big challenge because the programmed assembly of architectures such as $\mathbf{1}$ with co-axial n- and p-semiconducting π -stacks from π -basic and π -acidic aromatics is unfavorable (Figure 3). Oligomers of complementary aromatics such as π -

 $_{170}$ acid 2 and $\pi\text{-base}$ 3 prefer to undergo aromatic donor-acceptor interactions and form charge-transfer complexes such as double helix 4 instead. 14

The multichromophoric hybrids 5 self-assemble into π stack nanoarchitectures 6 with SHJ-like characteristics (Figure 175 4).15 Hybrids 5 are composed of a central tetraphenylporphyrin (TPP) donor that is surrounded by four perylenediimide (PDI) acceptors. To self-assemble into nanoparticles 6, PDIs from neighboring monomers are thought to interdigitate and form continuous face-to-face π -stacks. 180 This places the zinc porphyrins far enough apart to retain their ability to coordinate small ligands such as pyridine. PDI stacks are of interest because they are known as one of the few air-stable n-semiconductors. 16,17 TPP excitation in nanoparticle 6 causes PDI-TPP charge separation in 3.2 ps. Charge recombination to the resting state follows in 7.2 ns. High electron conductivity of the PDI stacks in 6 may account for the differences in CS and CR kinetics compared to monomer 5 (CS, 15 ps; CR 5.3 ns). Excitation of PDIs instead of TPPs is followed by energy transfer to the TPPs 190 (rather than electron transfer, see below).

The supramolecular trimer 7 self-assembles into left-handed helices that further self-assemble into right-handed supercoils. Trimer 7 contains a PDI acceptor in the middle. The acceptor-donor-acceptor (ADA) hydrogen-bonding motif of imides is used to bind a complementary DAD 2,4-diamino-1,3,5-triazine. This DAD domain is linked to a minimalist oligophenylvinyl (OPV) donor. Important for self-assembly, ADA-DAD hydrogen-bonding places the OPV donors in plane with the PDI acceptor. Support for SHJ architectures with π-200 stacked co-planar OPV-PDI-OPV arrays can be seen in the unusually fast CR in superhelical assemblies of 7. Thermal denaturation slows down CR, and less favorable assemblies obtained from covalent and deplanarized OPV-PDI-OPV

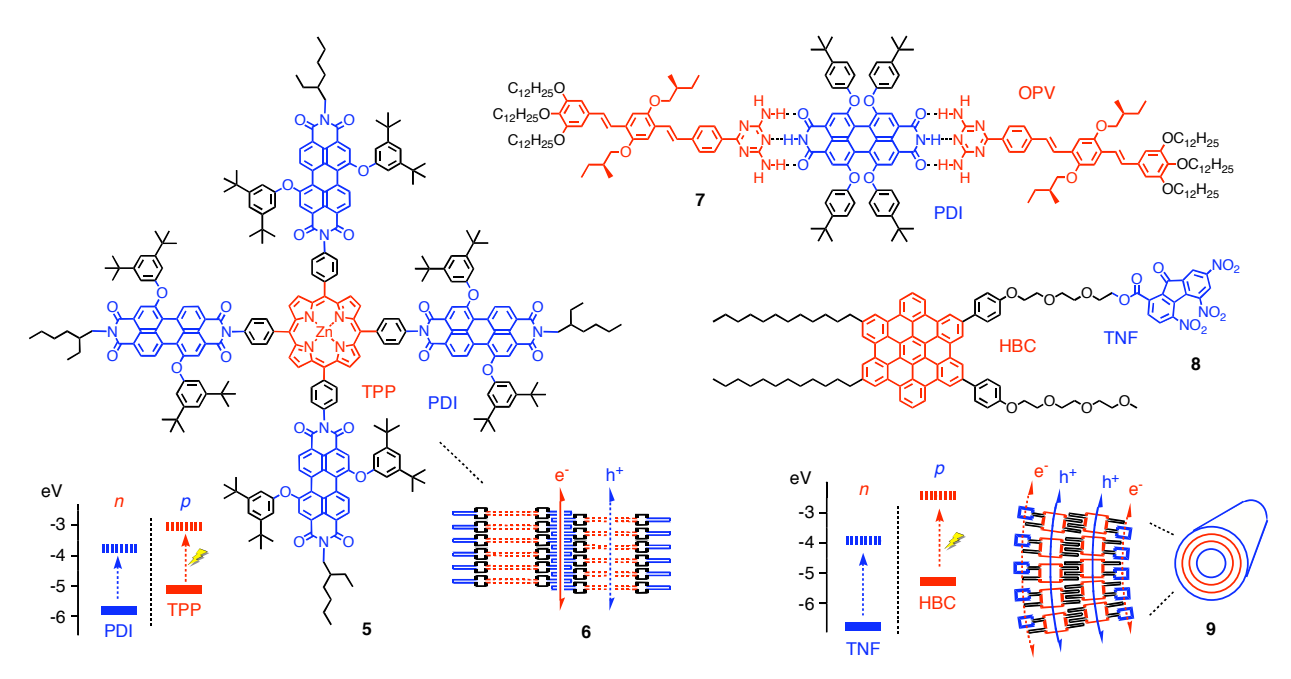


Fig. 4 Solution approaches toward SHJ architectures.

analogs recombine slower in assembled and disassembled ²⁰⁵ form. Contrary to the situation with **6**, high charge mobility in SHJ systems is here associated with accelerated CR. Poor diode behavior found upon spin coating **7** on the conducting surface was attributed to the wrong lateral orientation of the helices relative to the surface.

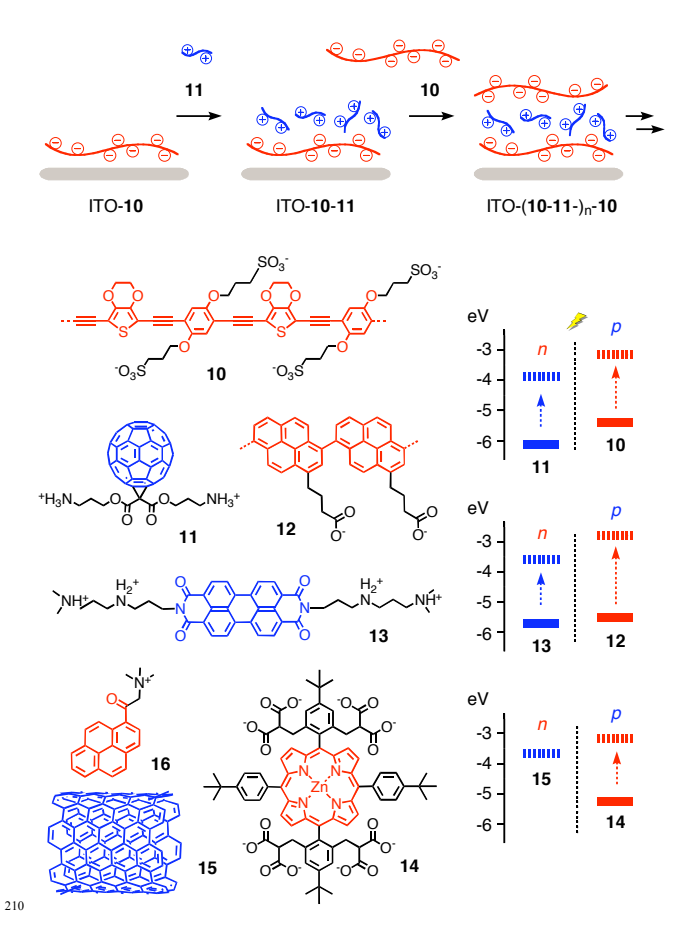


Fig. 5 Selected LBL assembly of donor-acceptor architectures.

Hexabenzocoronene (HBC) stacks rank among the best *p*-semiconductors (Figure 4).¹⁷ Amphiphilic HBCs such as **8** self-assemble under carefully optimized conditions into bilayer nanotubes such as **9**.¹⁹ In nanotube **9**, the trinitrofluorene (TNF) acceptors are added at inner and outer surface and form co-axial *n*-channels next to the HBC channel in the tube. This formal SHJ architecture generates photocurrent when spin-coated onto electrodes. Contrary to expectations for SHJs, mixed nanotubes with reduced TNF content give higher photocurrents.²⁰ Covalent cross-linking by ring-opening olefin metathesis (ROMP) is applicable to stabilize the active architectures.²¹

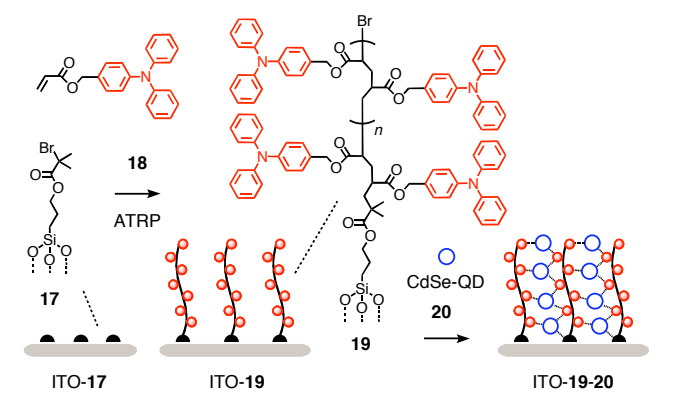
4 Oriented SHJs

225 Compared to self-assembly in solution, the creation of oriented SHJ architectures on solid substrates is much more challenging. Spin coating of preformed systems and other "top-down" approaches lack directionality and are thus intrinsically incompatible with the creation of oriented

230 architectures, not to speak of the installation of antiparallel redox gradients.

Layer-by-layer (LBL) assembly is the classical "bottomup" approach to oriented surface architectures (Figure 5). ²² In this approach, solid substrates such as ITO (indium tin oxide) ²³⁵ are dipped first into a solution of polyanions such as 10. ²³ Cooperative multivalent ion pairing attracts sufficient polyanion 10 not only to produce a polyanionic layer but also to cause surface charge inversion. The resulting anionic ITO-10 system is then dipped into solutions of di- or polycations ²⁴⁰ such as 11. The obtained, charge-inverted bilayers ITO-10-11 are incubated with polyanions 10, anionic ITO-10-11-10 with polycations 11, and so on. This process can be repeated many times to give thick films with ITO-(10-11-)_n LBL architectures.

LBL assembly has been used extensively for the creation of synthetic photosystems. Most popular are conjugated polymers as donors, including polyphenylethynyls, polythiophenes or mixed systems such as 10.23 Often, they are combined with charged fullerenes such as 11 as universal acceptors. The combination of oligopyrene donors 12 and PDI acceptors 13 is representative for possible variations that have been realized with the LBL theme.²⁴ Combined with standard TPP donors 14, a recent breakthrough with LBL photosystems introduces carbon nanotubes 15 as acceptors with exquisite conductivity. 25,26 Carbon nanotubes are solubilized and charged for LBL assembly with cationic pyrene donors 16 that bind to their aromatic surface by strong π , π -interactions.



 $_{260}$ Fig. 6 Notional SHJ photosystems made from polymer brushes.

The bell-shaped *J-L* curve of LBL architectures ITO-(10-11-)_n reveal an outstanding critical thickness of ~100 layers. The maximal $\eta_{\rm eff}=0.041\%$, claimed to be the best among LBL photosystems, is mainly limited by a disappointing FF=2650.31. This value is consistent with poor organization 11 as expected for LBL architectures 22 and as supported by characteristic nodular features on surfaces with a roughness up to 2.5 nm (rms). For comparison, LBL architectures ITO-(12-13-)_n feature a critical thickness of 10 layers and a 270 similarly bumpy surface with a roughness that, characteristically, increases from 2.6 to 4.7 nm (rms) with increasing thickness ($\eta_{\rm eff}$ and FF were not reported). 24 LBL architectures ITO-(14-15/16-)_n have a linear *J-L* curve up to 17 layers (*J-V* characteristics were not reported). 25

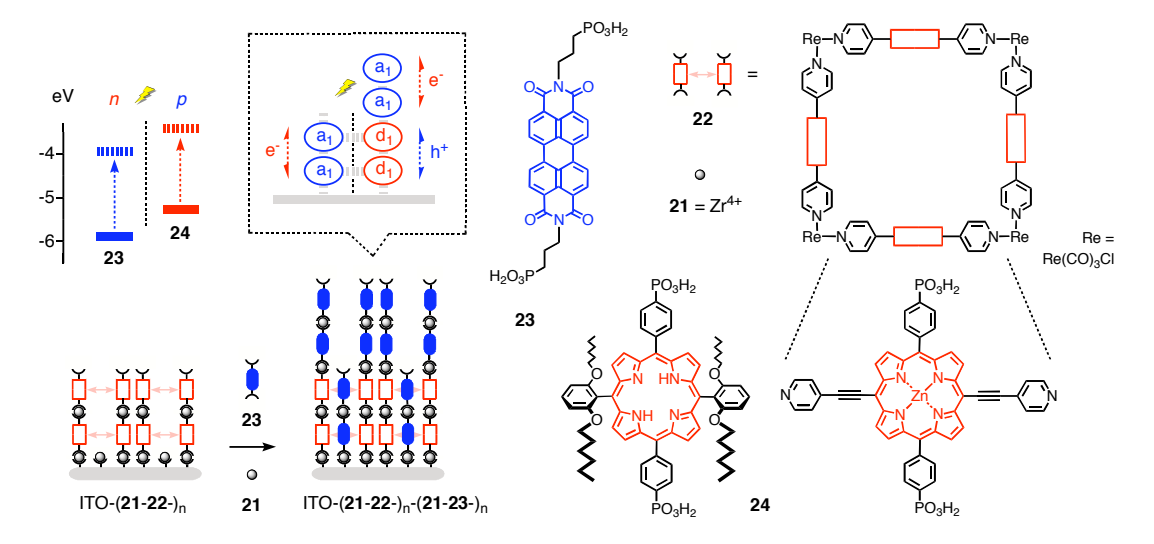


Fig. 7 Formal SHJ architecture obtained with porous arrays of porphyrin donors filled with PDI acceptors.

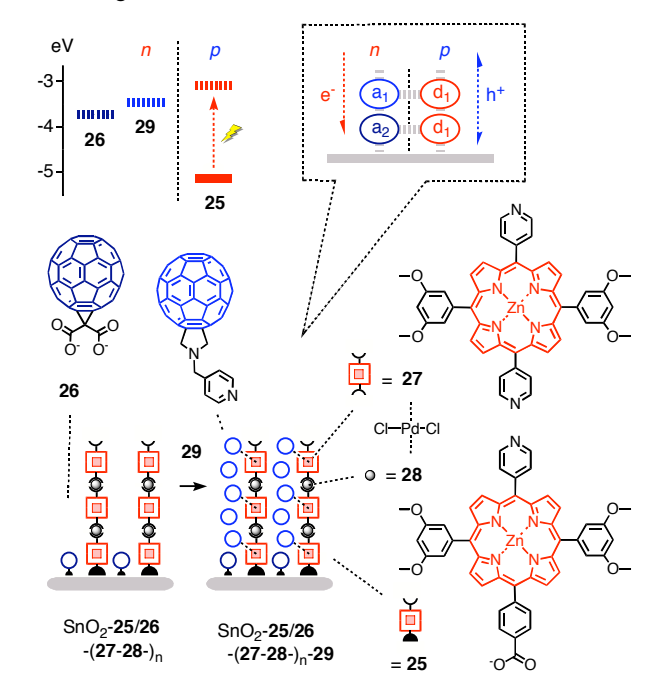
Easy accessibility to LBL architectures comes at the cost of poor organization and horizontal orientation of the adjacent nand p-semiconducting layers. Polymer brushes represent an inviting concept to reorient polymer backbones and achieve the vertical alignment desired for better charge collection at 280 the electrodes (Figure 6). 27,28 Polymer brushes are prepared by surface-initiated polymerization. The obtained close packing forces the polymers to align vertically to the surface. In the pioneering example focusing on SHJ architectures, ATRP (atom transfer radical polymerization) is used as most 285 popular method to make the brushes. Initiator 17 is grafted onto ITO surfaces to polymerize the triphenylamine acrylate 18 directly from ITO-17 in the presence of the standard Cu catalysts. The obtained ITO-19 brushes are then dipped into solutions of CdSe nanocrystals 20. Displacement of some of 290 their pyridine ligands by triphenylamines captures the CdSe nanocrystal acceptors along single polymer brush donors.

In polytriphenylamineacrylate brushes, the current density normal to the substrate is up to 3 orders of magnitude higher than in spin-coated films. Another increase in the current density by 3 orders of magnitude in the presence of nanocrystals in ITO-19-20 is due to the high conductivity of the latter and supports their complete infiltration into the brushes. Although high dark currents hinder standard characterization as formal SHJ photosystem, the general nature of the approach has high potential for future developments toward OMARG-SHJs.

Electropolymerization can be considered as special route toward polymer brushes.^{29,30} Electropolymerization of thiophenes together with semiconductor nanoparticles is expected to produce SHJ-type hybrid architectures that is very similar to the ATRP-derived ITO-19-20.²⁹

A very elegant and explicit approach toward oriented SHJ architectures uses zirconated ITO-21 surfaces to capture the four phosphonates at the bottom of porphyrin squares 22 ³¹⁰ (Figure 7). ³¹ Zirconation of the four phosphonates prepares for the binding of another porphyrin square. This ordered LBL process is repeatable and yields porous ITO-(21-22-)_n multilayers. The pores in ITO-(21-22-)_n are then filled by

repetitive LBL addition of PDI acceptors 23 and zirconium 315 cations 21 for reactivation of the terminal phosphonates. During the LBL infiltration of PDIs into the porphyrin squares, PDI acceptors are simultaneously captured on top of the porphyrin donors. Only the lower part of the obtained ITO-(21-22-)_n-(21-23-)_n architecture thus represents a formal 320 SHJ motif, where PDI donors are lined up vertically next to co-axial TPP acceptors, whereas the PDIs on top add a non-SHJ redox gradient.



 $\begin{tabular}{ll} \textbf{Fig. 8} & \textbf{Notional SHJ photosystems made from supramolecular polymer} \\ \textbf{325} & \textbf{brushes}. \\ \end{tabular}$

Elegant experiments have been conceived to support the existence of the designed architecture. Discontinuous PDI reducibility, for instance, provides excellent support that the PDIs really penetrate the porphyrin squares. Replacement of squares 22 with crowded porphyrins 24 gives similar

architectures. Both architectures afford linear *J-L* curves up to 8-10 layers. Action spectra demonstrate that both PDIs and TPPs contribute to photocurrent generation. *J-V* curves were not reported.

A recent ambitious approach combining aspects of several previous systems begins with carboxylate linker on tin oxide to produce a mixed monolayer of porphyrin donors 25 and fullerene acceptors 26 (Figure 8).³² The porphyrins in SnO₂-25/26 are activated by adding palladium propagators 27 to the 340 pyridine ligand. Incubation of the obtained SnO₂-25/26-27 with dipyridine porphyrin 28 followed by reactivation with Pd 27 gives SnO₂-25/26-27-28-27. Repeated ordered LBL incubation with 28 and 27 produces supramolecular metalloporphyrin brushes SnO₂-25/26-(27-28-)_n. To infiltrate 345 a coaxial string of donors, fullerenes 29 are added with the expectation that their pyridine tail acts as axial ligand to the zinc porphyrins. The elegant combination of peripheral and central porphyrin coordination chemistry in SnO₂-25/26-(27-28-)_n-29 affords a formal SHJ architecture with strings of 350 porphyrin acceptors that grow from the surface and are lined by coaxial strings of fullerene acceptors. The lowered LUMO of fullerene 26 compared to fullerene 29 adds a formal redox gradient to the *n*-channel.

J-L curves of SnO_2 -25/26-(27-28- $)_n$ -29 reveal a critical sistematical thickness of 5 layers with an incident photon-to-current efficiency IPCE = 21% at J_{max} . Photocurrent decrease after more than 5 layers of depositions coincides with inhibited growth of the system. This suggests that reduced growth mainly accounts for photocurrent decrease. At J_{max} with 5 layers, the addition of pyridine fullerenes 29 nearly doubles the photocurrent density, whereas fullerenes with phenyls in place of pyridines cause only an increase of about 10%. AFM images reveal reasonably smooth surfaces, with surface roughness increasing with increasing number of layers in the 365 presence and the absence of fullerenes (J-V characteristic were not reported).

Zipper assembly of rod-stack architectures such as Au-30-(31-32-)_n has been introduced as metal-free, all-organic approach to SHJ photosystems (including OMARG-SHJs, see Zipper architectures are assembled from multichromophoric donor-acceptor hybrids beginning with the short POP-B initiator 30 (Figure 9. POP: p-oligophenyl). The disulfide at one end is introduced to bind covalently to gold, negatively charged blue NDIs B are placed along the short 375 rigid-rod POP scaffold to avoid non-specific interaction with gold. The formal Au-30 monolayer is then exposed to POP-B propagator 31. Driven by π,π -stacking, intrastack hydrogen bonding and interstack ion pairing, 34,35 the lower half of the blue and cationic NDIs of 31 are expected to π -stack with the 380 anionic NDI acceptors of 30, whereas the upper half remains free as "sticky end" to zip up with the complementary anionic POP-B propagator 32. Repeated incubation with cationic 31 and anionic 32 gives zipper Au-30-(31-32-)_n.

Au-30-(31-32-)_n is designed to feature π -stacks formed by interdigitating aromatic planes from neighboring scaffolds along strings of interdigitating rigid rods. This architecture excels with operational inter- and intralayer recognition motifs as well as the co-axial alignment of *n*-semiconducting NDI stacks next to *p*-semiconducting POP rods. However,

photo induced CS (PCS) between NDI stacks and POP rods is not possible with Au-30-(31-32-)_n because the HOMO of blue NDIs B is above that of POPs. As with the special pair of chlorophylls in the heart of biological photosystems, this gives a donor-acceptor-free system with symmetry-breaking
 PCS between blue NDIs B as only way to proceed, one B being reduced to B⁻ and one B being oxidized to B⁺, with minimal losses of energy.
 In this situation, both hole and electron would move in adjacent NDI stacks, with POPs serving as rigid-rod scaffolds only without any functional
 role.

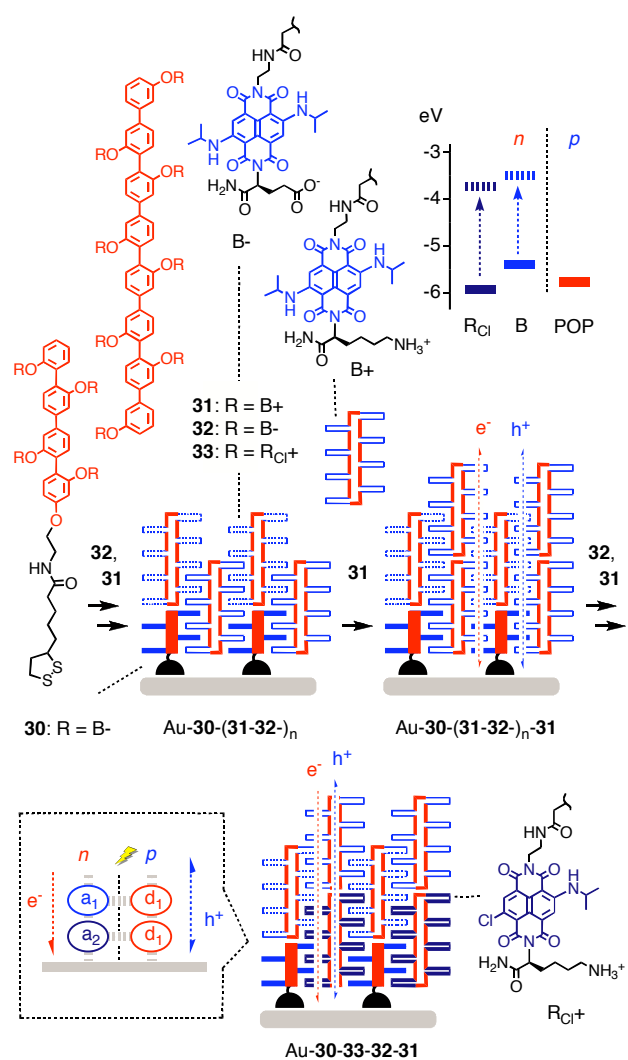


Fig. 9 Zipper assembly of notional SHJ architectures.

According to the kinetics of the transient absorption of the NDI⁻ radical anion, monomeric **31** is capable of ultrafast, symmetry-breaking PCS. PCS lives for 60 ps in monomeric **31** and 400 ps in self-assembled tetramers in lipid bilayer membranes. ^{35,36} Zipper architectures Au-**30**-(**31-32**-)_n exhibit linear *J-L* curves up to 10 layers. ³³ Capping of the sticky ends in Au-**30-31** with short **30** cleanly inhibits further increases in photocurrent generation, as does replacement of the cationic propagator **31** with disorganizing polylysines. Mini-zippers with biphenyl initiators and *p*-quaterphenyl propagators generate less photocurrent and have bell-shaped *J-L* curves

with $J_{\rm max}$ at 10 layers, corresponding to 5 layers with standard ⁴¹⁵ Au-30-(31-32-)_n zippers. ³⁷ Consistent with high organization of zipper architectures, the "non-ohmic" J-V curve of Au-30-31-32-31 was characterized by FF = 0.42, a quite remarkable value for gradient-free architectures with an expected thickness of ~6 nm only. ³⁸

To activate both n- and p-semiconductor channels in notional rod-stack POP-NDI zipper SHJ architectures, POP-R_{Cl} donor-acceptor hybrids were included.³⁸ With the HOMO of R_{Cl} lying below that of POP, PCS by rod-stack electron transfer from POP donors to R_{Cl} acceptors is possible in this 425 case. PCS with POP-R_{Cl} dyads 33 is correspondingly longlived, with decay components reaching into the ns range. Consistent with rod-stack PCS, that is the formation of notional SHJ architectures, the action spectra of mixed zippers show that photocurrent generation by R_{Cl} exceeds that by B 430 dramatically. The J-V curve of Au-30-33-32-31 excels with high $V_{\rm OC}$ and an outstanding FF = 0.55, whereas the isomeric Au-30-31-32-33 with the reversed redox gradient in the NDI stack has a nearly "ohmic" FF = 0.31 and lower $V_{\rm OC}$. This difference in FF between the system with constructive redox 435 gradients to guide the electrons to the gold surface and that with destructive ones driving the electron away from the surface demonstrate how B-R_{Cl} gradients in POP-NDI zipper architectures matter for function. Au-30-33-32-31, containing NDIs of red and blue color, can thus be considered as 440 minimalist prototype of a formal OMRG-SHJ photosystem.

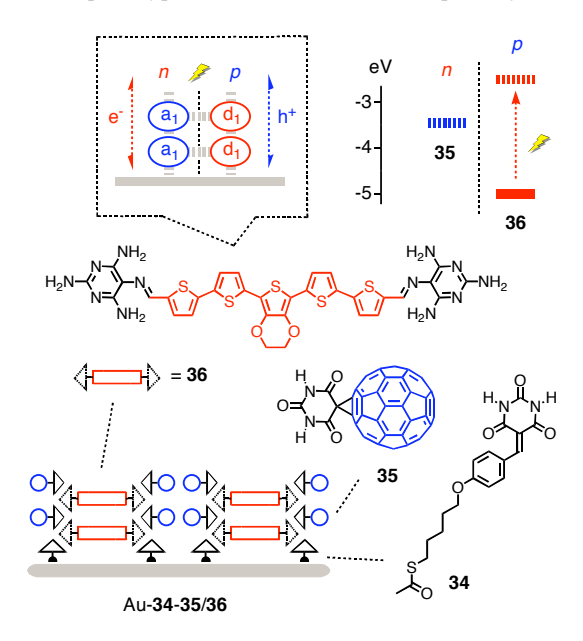


Fig. 10 Toward SHJ systems with H-bonding network architectures.

An inspired approach toward all-organic SHJ architectures ⁴⁴⁵ is under development with systems such as Au-34-35/36 (Figure 10). ³⁹ This approach has much future potential because it introduces the rich supramolecular chemistry of hydrogen-bonding network architectures. Best known for the self-assembly of supramolecular rosettes and tapes, ^{40,41} barbiturate derivatives as in fullerene acceptors 35 are popular sectors that offer two linear acceptors-donor-acceptor (ADA) triads in a 60° angle. They pair with the matching DAD triads

in the 60° sector of melamines in oligothiophenes 36. For their surface-initiated supramolecular polymerization, both components are deposited together on gold coated with monolayers of barbiturate derivative 34. Photocurrents generated with 35 and 36 are higher in the presence of initiator 34 than in the presence of methylated analogs and barbiturate initiators.

460 5 Redox Gradients

In ideal OMARG-SHJs, oriented SHJs would be equipped with antiparallel redox gradients to move electrons and holes in opposite directions to their final destination. Although today's small collection of formal SHJs contains examples with traces of one unidirectional two-component gradient, significant SHJ cascades remain to be realized, not to speak of two antiparallel gradients in *n*- and *p*-channels. However, several photosystems with quite significant redox gradients have been prepared by top-down approaches.

For example, vapor deposition of layers of first tetraceno [2,3-b]thiophene donors followed by bifunctional copper phthalocyanines and fullerene acceptors gives trilayer photovoltaic cascade devices with increased $V_{\rm OC}$. Full increase in $V_{\rm OC}$ occurs only with phthalocyanine layers thicker than 5 nm. This finding is very important because it demonstrates that $V_{\rm OC}$ in cascade architectures is determined not by the smallest HOMO-LUMO differences but by either neighboring or perhaps even maximal HOMO-LUMO differences. Redox gradients can thus be considered as promising approach to increase $V_{\rm OC}$.

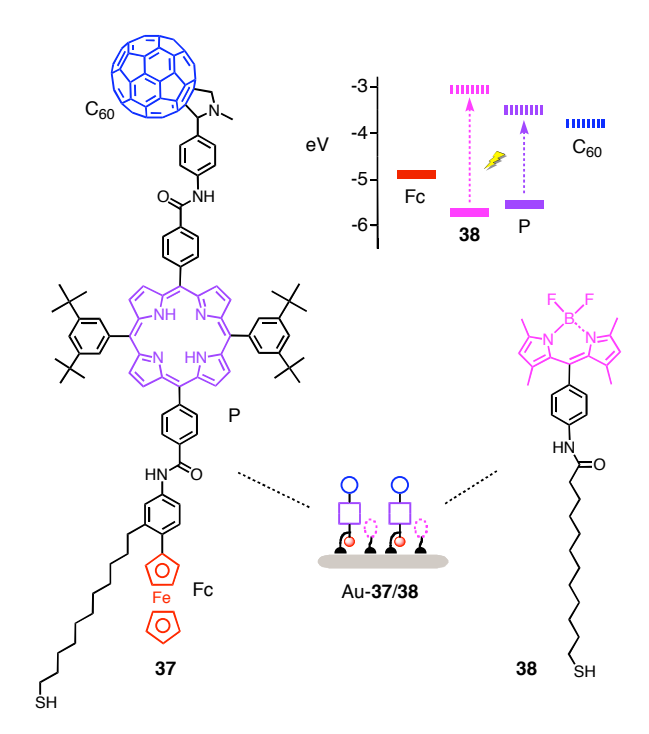


Fig. 11 Mixed SAM photosystems to combine redox gradients with light harvesting.

The covalent construction of redox gradients has been explored quite extensively with self-assembled monolayers

(SAMs). 42,43 An excellent example for an advanced system is the formation of mixed SAMs with fullerene-porphyrin-ferrocene triad **37** and boron dipyrrin **38** as energy donor on 490 the gold surface (Figure 11).

SAMs are simple enough to explore the more complex systems accessible with biological scaffolds. Judicious multiple cystein mutation, for example, can produce SAMs with bioengineered photosystems for photocurrent generation. SAMs from DNA double helices such as **39** and **40** are perfect to explore the importance of π-stack conductivity for photocurrent generation (Figure 12). To do so, duplexes **39** and **40** are terminated with a naphthaleneimide (NI) acceptor on one side and a thiol on the other side for covalent capture on gold.

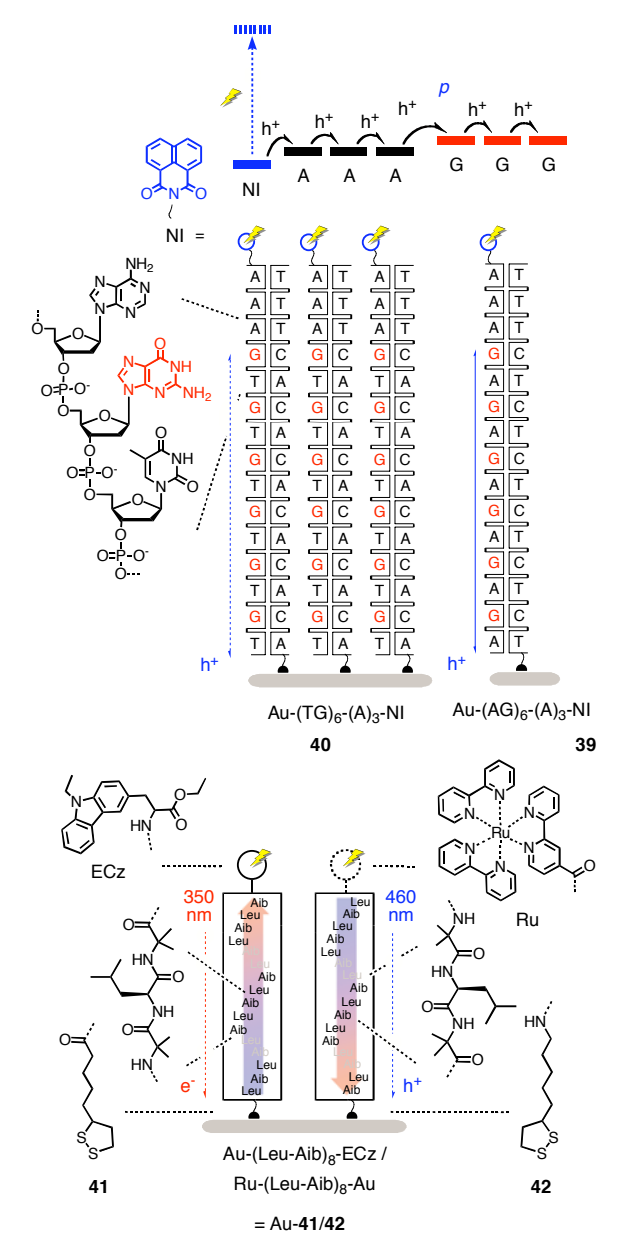


Fig. 12 DNA duplexes and peptide α-helices as bioinspired scaffolds to sos elucidate the importance of conductivity and macrodipoles for photocurrent generation, respectively.

With constant A_3 spacers between NI acceptors and G donors, DNA **39** with GA repeats generates significant photocurrent, whereas DNA **40** with GT repeats is inactive. This difference originates from the difference in conductivity of GA and GT repeats, the former being sufficient to remove the hole before charge recombination of the NI $^-$ -G $^+$ - ion pair occurs. Elongation of the A_3 to A_4 spacers results in nearly the same photocurrent generation with GT and GA conductors, whereas shortening to A_2 spacers inactivates also the systems with GA conductors. Single pair mismatches in the conductor part of the DNAs are detectable as reduction in photocurrent.

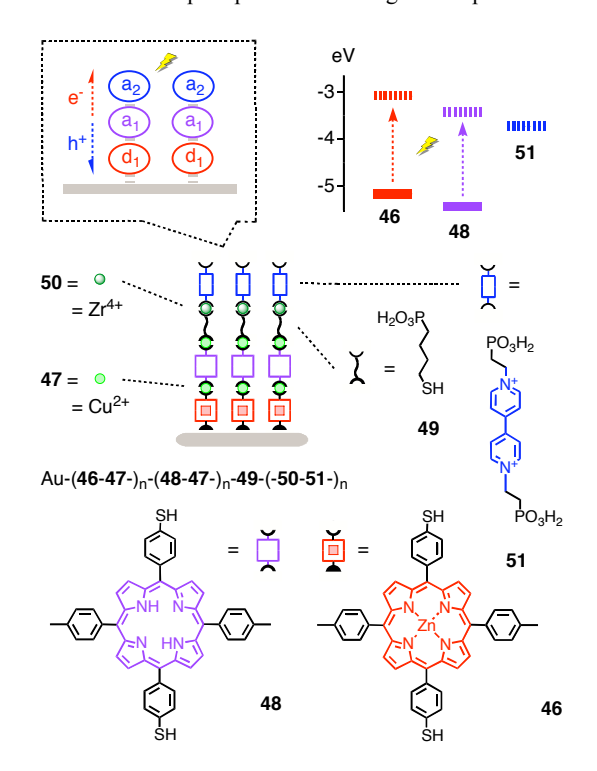
Fig. 13 All-organic LBL photosystems with oriented redox gradients.

α-Helical peptide scaffolds are perfect to explore the usefulness of macrodipoles to control the directionality of electron transfer. 46,47 The minimalist helices 41 and 42 are 525 made from a simple hydrophobic Leu-Aib repeat to minimize interference from competing secondary structures. In helix 41, a disulfide is added at the N-terminus for covalent linking to gold and an ECz chromophore is added at the C-terminus. In helix 42, however, the disulfide is at the C-terminus and a Ru chromophore at the N-terminus. In mixed SAMs on gold, the macrodipole of helix 41 points toward the ECz chromophore, whereas the macrodipole of helix 42 points away from the Ru chromophore. As a result, excitation of the ECz chromophore at 350 nm causes electron transfer to the gold surface, whereas excitation of the Ru chromophore at 460 nm causes hole transfer to the gold surface. The extraordinary result is a photodiode switch, where, due to the antiparallel orientation of the α-helical macrodipole,

540 irradiation at 350 nm anodic photocurrents.

Despite relatively low conductivity due to the lack of molecular level organizations, LBL assembly remains the supramolecular approach of choice to photosystems with more significant redox gradients (Figure 13). In a pioneering 545 model, anionic fullerene dendrimers 43 on a ITO surface are covered with cationic porphyrin acceptors 44, which in turn are covered with anionic zinc porphyrin donors and cationic ferrocenes as final donors. 48 Action spectra demonstrate that ITO-43-44 produces very little, ITO-43-44-14 more and ITO-550 43-44-14-45 most photocurrent. At the absorption maximum of the porphyrins, the final system is with an IPCE = 1.6% 108-times more active than the simple fullerene-porphyrin bilayer Au-43-44.

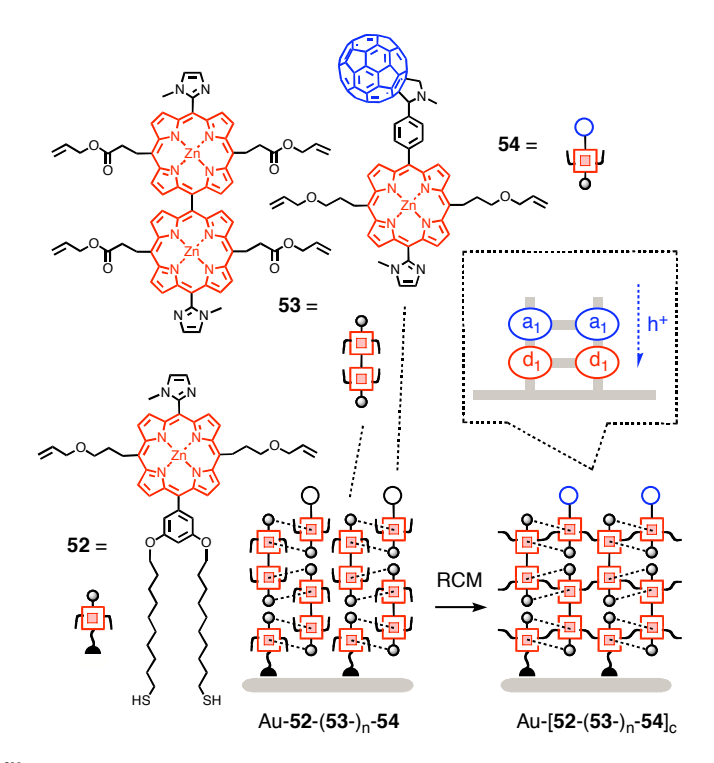
An early and seminal breakthrough toward ordered, SHJ-555 compatible (Figure 8) coordination networks with porphyrins focuses on the programmed assembly of oriented redox gradients (Figure 14). 49 Dithiolated zinc porphyrin donors 46 are deposited on gold and activated by coordination to copper 47 for the repetitive ordered LBL build up of a donor domain 560 Au-(46-47)_n. On top of this domain, a bifunctional domain is added by repetitive exposure to dithiolate porphyrin acceptors **48** and copper **47**. On the resulting $Au-(46-47-)_n-(48-47-)_n$ the alkyl converter 49 with a thiol at one and a phosphonate at the other end is added. The phosphonate at the surface of Au- $_{565}$ (46-47-)_n-(48-47-)_n-49 is the starting point to build an acceptor layer by repetitive incubation in solutions of zirconium 50 and diphosphonated viologen acceptor 51.



An ordered LBL metallo-photosystem with oriented redox Fig. 14 gradients.

Compared to similar systems, the J-V curves of Au-(46-47- $)_n$ -(48-47- $)_n$ -49-(50-51- $)_n$ shows outstanding characteristics.

irradiation at 460 nm reversibly generates cathodic and 575 Fill factors increase from FF = 0.31 for Au-(48-47-)₃-49-(50-51-)₃ with a weak redox gradient to FF = 0.58 for Au-(46-47- $)_3$ -49-(50-51-)3 with a strong redox gradient and a similar FF for the full cascade in Au- $(46-47-)_2-(48-47-)_1-49-(50-51-)_3$. The $V_{\rm OC}$ of full cascades Au- $(46-47-)_2-(48-47-)_1-49-(50-51-)_3$ 580 is as large as that of Au- $(48-47-)_3-49-(50-51-)_3$ with a weak redox gradient and larger than that of Au-(46-47-)3-49-(50-51-)₃ with a strong gradient. This observation is in agreement with the earlier speculation that $V_{\rm OC}$ in redox cascades are determined by neighboring or maximal rather than minimal 585 HOMO-LUMO differences. As a result, the overall chargeseparation quantum yield for full redox cascade is with 3.5% larger than with photosystems missing one component (2.4%).



Combining coordinative surface-initiated supramolecular polymerization (SISP) with covalent capture by ring-closing olefin metathesis (RCM) to stabilize thick and ordered porphyrin architectures with terminal fullerene acceptors.

An elegant approach focusing on the combination of surface-initiated supramolecular polymerization interdigitatng mutual porphyrin coordination with covalent capture addresses the challenge of how to build thick films without losing the long-range organization (Figure 15).50 The construction begins with the deposition of the doubly thiolated zinc porphyrin initiator 52 on gold. To Au-52, the dimeric porphyrin 53 is added. One methylimidazole ligand of propagator 53 binds as axial ligand to the zinc porphyrin 52, whereas the methylimidazole ligand of initiator 52 back-binds as axial ligand of the zinc porphyrin 53. This mutual, doubly coordinative binding not only strengthens the interaction but also firmly orients propagator 53 with regard to initiator 52. The second zinc porphyrin and methylimidazole ligand of propagator 53 remains free at the surface of Au-52-53 to 610 capture the first porphyrin of the next propagator 53, and so

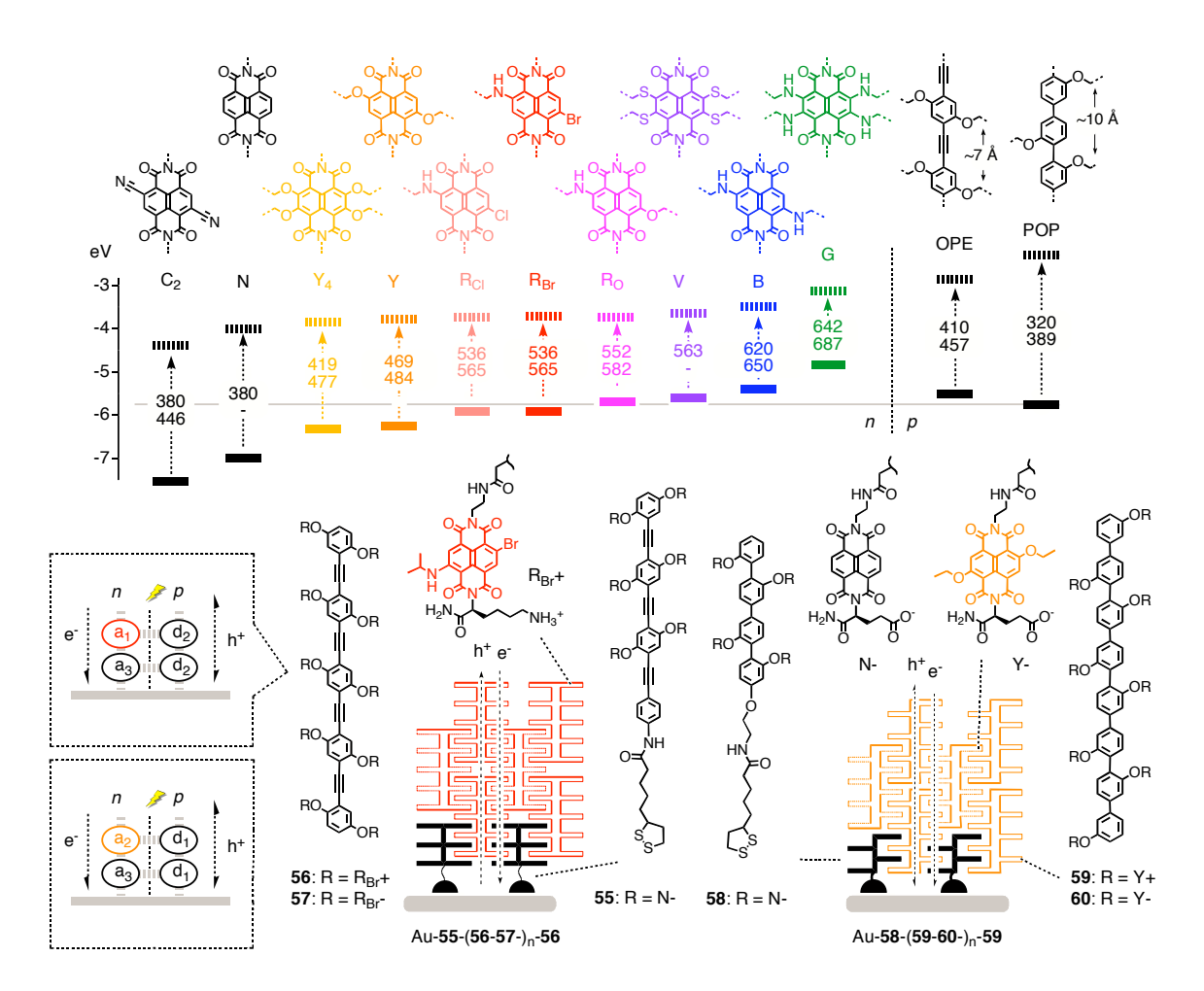


Fig. 16 Frontier orbital energy levels of NDIs (general structures C₂-G), OPEs and POPs (solid lines, HOMO; dashed lines, LUMO; dashed arrows, absorption of light; with wavelength (nm) of maximal absorption (top) and emission (bottom) and structure of POP-Y and OPE-R_{Br} dyads **55-60** as well as their zipper assemblies.

on. Once the surface-initiated supramolecular polymerization (SISP) stops, Grubbs catalyst is added to crosslink all porphyrins by ring-closing olefin metathesis (RCM). After RCM, SISP with propagator 53 is operational again, and RCM and SISP with propagator 53 can be repeated to build, according to linear SPR *J-L* curves, films as thick as 7 nm in 5 cycles. Coordinative capping with porphyrin 54 carrying a terminal fullerene acceptor more than doubles the generated photocurrent. *J-V* curves show nearly ohmic behavior.

620 6 Multicolor Systems

In ideal OMARG-SHJs, the coaxial n- and p-semiconducting pathways are not only equipped with antiparallel redox gradients but also contain chromophores that absorb light over and beyond the entire visible range. For the programmed 625 assembly of multicolor architectures on surfaces, this bandgap modulation must occur without global changes in structure. Multicolor systems are conceivable with many chromophores. Marvelous examples for rainbow collections include besides NDIs also the Alexa Fluor series, fluoresceins, BODIPYs, azobenzenes, porphyrinoids or triangular dehydrobenzo[12]annulenes.53-57 As long as multicolor systems are used for energy transfer only, bandgaps matter but absolute frontier orbital energies are irrelevant. Such energy cascades have been built in many variations to harvest light. Highlights reach from filled and oriented zeolites⁵⁶ to bioengineered tabacco mosaic viruses.⁵⁷ Tandem solar cells are simple engineering approach to multicolor photosystem.⁵⁸ Beyond supramolecular chemistry, quantum dots appear attractive for energy transfer in multicolor photovoltaics, whereas their use to construct redox gradients seems less promising because decreasing HOMO with increasing LUMO levels produce low-energy electron traps.^{59,60}

For compatibility with OMARG-SHJs, multicolor chromophore collections must possess many challenging characteristics. NDIs⁶¹⁻⁶⁵ are ideal candidates because they offer the spectacular combination of 1) decreasing HOMO/LUMO with increasing bandgap, ^{10,35,62-64} 2) *n*-semiconductivity, ^{16,65} 3) π-acidity, ¹³ 4) planarity, 5) global structural preservation, 6) compactness ("atom efficiency") and 7) synthetic accessibility (Figure 16).

NDIs cover the primary colors by replacing only a few atoms. 61-64 Introduction of two alkoxy substituents into the NDI core converts the colorless parent structure N into the yellow, green-emitting fluorophores Y. Formal substitution of

655 one oxygen atom in Y with a nitrogen atom gives the red, orange-emitting R_O. Substitution of the second alkoxy with an alkylamino π -donor gives the blue, red-emitting minimalist chlorophyll mimic B. Many more bandgaps are accessible with NDIs having two to four electron-donating (amines, 660 ethers, sulfides, halogens, etc) and accepting substituents (cyano, etc) in the core. 61-64 Among other NDI characteristics, the fact that their face-to-face π -stacks represent one of the few air-stable molecular nsemiconductors deserves particular attention. 16,17 Although 665 easier to synthesize, the homologous PDI⁶⁶ series appears less suitable to build OMARG-SHJs because core substitution twists the aromatic plane, may hinder ordered stacking and thus reduce the conductivity of potential MRG stacks. In addition, the planar NDIs are more compact and provide 670 access to high-energy photons.

7 Toward OMARG-SHJs

Rod-stack zipper assembly could potentially serve as a platform to build OMARG-SHJ architectures (Figures 9 and 16). Toward this end, oligophenylethynyls (OPEs) are examined as alternative and accompanying rigid-rod scaffolds to the original POPs. Compared to POPs, OPEs are attractive because they can be planarized, conduct holes better and absorb more visible light. Moreover, their repeat distance matches with ~7 Å the repeat of π-stacks. The mismatched 10 Å repeat of POPs has been shown to cause hyperbolidal collapse into more helical architectures. Most importantly for OMARG-SHJs, the HOMO of OPEs lies above that of POPs.

Zipper assembly of OPE-NDI architectures Au-55-(56-57-)_n, is achieved by repetitive dip-wash procedures as described above for POP zippers.⁶⁷ OPE-NDI zippers Au-55-(56-57-)_n excel with *FF* = 0.61, a critical thickness of 20 layers, increasing (rather than decreasing) surface smoothness with oincreasing thickness, and perfect responsiveness to functional tests such as zipper capping and LBL assembly without initiator 55. The mismatched POP-NDI zipper homologs have a critical thickness of ~8 layers, rougher surfaces and, in the case of brominated NDIs only, poor responsiveness to functional probes. These differences provide experimental support that zipper architectures exist and that topological matching matters.

Action spectra of final Au-55-(56-57-)_n indicate that OPEs are planarized and contribute to photocurrent generation.

Consistent with the formation of SHJs, transient absorption spectroscopy demonstrates that OPE excitation is followed by electron (rather than energy) transfer to the NDI acceptors in the femtosecond timescale.

The yellow POP-Y zippers Au-58-(59-60-)_n complement root red OPE-R_{Br} zippers Au-55-(56-57-)_n. In POP-Y zippers Au-58-(59-60-)_n, the optoelectronic matching of Y acceptors with POP donors is correctly reflected in maximal photocurrent generation compared to the less favorable red POP-R_{Cl} and blue POP-B zippers. Long-lived PCS in POP-Y dyads in the nanosecond timescale is in agreement with this interpretation. High π -acidity, very smooth surfaces, high FF

= 0.53 in J-V curves and high critical thickness of ~20 layers in J-L curves of POP-Y zippers Au-58-(59-60-)_n reveal origin and existence of highly ordered rod-stack SHJ architectures.

With unsubstituted NDI acceptors near the gold surface, both POP-Y zipper Au-58-(59-60-)_n and OPE-R_{Br} zipper Au-55-(56-57-)_n have a formal redox gradient in the n-semiconducting channel. Placed on top of each other, mixed POP-Y and OPE-R_{Br} zippers would give formal OMARG-720 SHJs, where Y acceptors in the NDI stack can accept electrons from R_{Br} donors and direct them to the bottom of the multilayer architecture, whereas p-semiconducting strings of OPEs can accept holes from strings of POPs underneath and direct them to the top.

725 8 Epilogue

This tutorial review introduces the concept of OMARG-SHJ architectures as bioinspired ideal photosystems and summarizes recent progress made to get there. The overall impression is that the decisive challenge concerns the question of how to build "bottom-up" and with molecular-level precision on solid grounds. Whereas a broad palette of parameters influences the final phenotype, the key to success thus seems to be at the interface of synthetic organic, supramolecular, polymer and analytical surface chemistry. Promising and emerging methods employed and conceived to tackle this challenge include LBL assembly, zipper assembly, surface-initiated polymerization (polymer brushes), surfaceinitiated supramolecular polymerization, electropolymerization and covalent capture. Much potential can be seen in the development of multicolor donor-acceptor systems beyond current preferences such as porphyrins and fullerenes. Expectations such as high critical thickness, fill factors and open circuit voltage for OMARG-SHJ architectures are supported by several examples. Access to these characteristics would find broad applicability in molecular optoelectronics, including high-efficiency solar cells or logic devices. Although it remains to be seen whether or not OMARG-SHJs ultimately live up to these expectations, the road to get there promises in any case to be everything 750 else than boring.

Acknowledgments

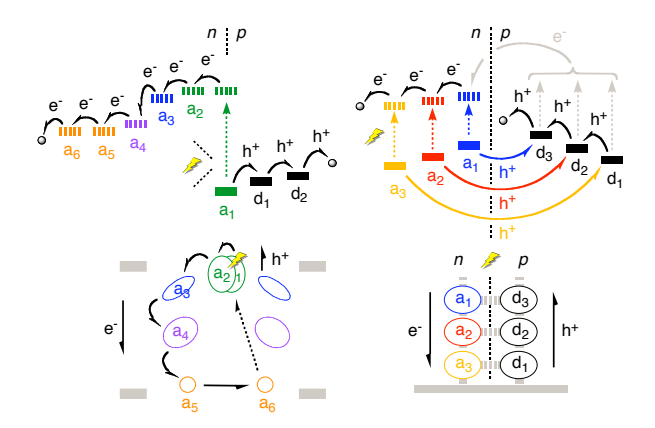
This work was supported by the University of Geneva and the Swiss NSF. JM is a fellow of the Roche Research Foundation. Sincere apologies to all colleagues whose work could not be covered because of limitations in space and scope.

References

- J. Deisenhofer and H. Michel, *Science*, 1989, **245**, 1463-1473.
- N. Nelson and A. Ben-Shem, Nat. Rev. Mol. Cell Biol., 2004, 5, 971-982.
 - 3 C. W. Tang, Appl. Phys. Lett., 1986, 48, 183-185.
 - 4 G. Yu, J. Gao, J. C. Hummelen, F. Wudl and A. J. Heeger, *Science*, 1995, **270**, 1789-1791.
- B. C. Thompson and J. M. J. Fréchet, *Angew. Chem. Int. Ed.*, 2008,
 47, 58-77.
- S. Gnes, H. Neugebauer and N. S. Sariciftci, *Chem. Rev.*, 2007, 107, 1324-1338.

- 7 C. Ma, M. Fonrodona, M. C. Schikora, M. M. Wienk, R. A. J. Janssen and P. Bäuerle, Adv. Funct. Mater., 2008, 18, 3323–3331.
- 770 8 J.-F. Eckert, J.-F. Nicoud, J.-F. Nierengarten, S.-G. Liu, L. Echegoyen, N. Armaroli, F. Barigelletti, L. Ouali, V. Krasnikov and G. Hadziioannou, J. Am. Chem. Soc., 2000, 122, 7467-7479.
 - V. Balzani, M. Venturi and A. Credi, Molecular Devices and Machines, Wiley-VCH, Weinheim, 2003.
- 775 10 R. S. K. Kishore, O. Kel, N. Banerji, D. Emery, G. Bollot, J. Mareda, A. Gomez-Casado, P. Jonkheijm, J. Huskens, P. Maroni, M. Borkovec, E. Vauthey, N. Sakai and S. Matile, submitted.
 - 11 F. Yang, M. Shtein and S. Forrest, Nat. Mater., 2005, 4, 37-41.
 - 12 S. Sista, Y. Yao, Y. Yang, M. L. Tang and Z. Bao, *Appl. Phys. Lett.*, 2007, **91**, 223508/1-223508/3.
 - 13 J. Mareda and S. Matile, Chem. Eur. J., 2009, 15, 28-37
 - 14 G. J. Gabriel and B. L. Iverson, J. Am. Chem. Soc., 2002, 124, 15174-15175.
- 15 T. Van der Boom, R. T. Hayes, Y. Zhao, P. J. Bushard, E. A. Weiss and M. R. Wasielewski, J. Am. Chem. Soc., 2002, 124, 9582-9590.
- 16 B. A. Jones, A. Facchetti, M. R. Wasielewski and T. J. Marks, J. Am. Chem. Soc., 2007, 129, 15259-15278.
- 17 J. M. Warman, M. P. de Haas, G. Dicker, F. C. Grozema, J. Piris and M. G. Debije, *Chem. Mater.*, 2004, 16, 4600-4609.
- 790 18 F. Würthner, Z. Chen, F. J. M. Hoeben, P. Osswald, C.-C. You, P. Jonkheijm, J. Herrikhuyzen, A. P. H. J. Schenning, P. P. A. M. van der Schoot, E. W. Meijer, E. H. A. Beckers, S. C. J. Meskers and R. A. J. Janssen, J. Am. Chem. Soc., 2004, 126, 10611-10618.
- 19 Y. Yamamoto, T. Fukushima, Y. Suna, N. Ishii, A. Saeki, S. Seki, S. Tagawa, M. Taniguchi, T. Kawai and T. Aida, *Science*, 2006, 314, 1761-1764
- 20 Y. Yamamoto, T. Fukushima, A. Saeki, S. Seki, S. Tagawa, N. Ishii, and T. Aida, J. Am. Chem. Soc., 2007, 129, 9276-9277.
- 21 T. Yamamoto, T. Fukushima, Y. Yamamoto, A. Kosaka, W. Jin, N. Ishii and T. Aida, *J. Am. Chem. Soc.*, 2006, **128**, 14337-14340.
- 22 G. Decher, Science, 1997, 277, 1232-1237.
- 23 J. K. Mwaura, M. R. Pinto, D. Witker, N. Ananthakrishnan, K. S. Schanze and J. R. Reynolds, *Langmuir*, 2005, 21, 10119-10126.
- 24 L. Zhao, T. Ma, H. Bai, G. Lu, C. Li and G. Shi, *Langmuir*, 2008, **24**, 4380-4387.
- 25 D. M. Guldi, G. M. A. Rahman, M. Prato, N. Jux, S. Qin, and W. Ford, Angew. Chem. Int. Ed., 2005, 44, 2015-2018.
- 26 D. M. Guldi, J. Phys. Chem. B, 2005, 109, 11432-11441.
- G. L. Whiting, H. J. Snaith, S. Khodabakhsh, J. W. Andreasen, D. W.
 Breiby, M. M. Nielsen, N. C. Greenham, R. H. Friend and W. T. S. Huck, *Nano Lett.*, 2006, 6, 573-578.
- 28 H. J. Snaith, G. L. Whiting, B. Sun, N. C. Greenham, W. T. S. Huck and R. H. Friend, *Nano Lett.*, 2005, 5, 1653-1657.
- R. C. Shallcross, G. D. D'Ambruoso, B. D. Korth, H. K. Hall, Z.
 Zheng, J. Pyun and N. R. Armstrong, J. Am. Chem. Soc., 2007, 129, 11310-11311.
- 30 E. Hwang, K. M. N. de Silva, C. B. Seevers, J.-R. Li, J. C. Garno and E. E. Nesterov, *Langmuir*, 2008, **24**, 9700-9706.
- A. B. F. Martinson, A. M. Massari, S. J. Lee, R. W. Gurney, K. E.
 Splan, J. T. Hupp and S. T. Nguyen, *J. Electrochem. Soc.*, 2006, 153, A527-A532.
 - 32 A. Kira, T. Umeyama, Y. Matano, K. Yoshida, S. Isoda, J. K. Park, D. Kim and H. Imahori, *J. Am. Chem. Soc.*, 2009, 131, 3198-3200.
- N. Sakai, A. L. Sisson, T. Bürgi and S. Matile, J. Am. Chem. Soc.,
 2007, 129, 15758-15759.
- 34 P. Talukdar, G. Bollot, J. Mareda, N. Sakai and S. Matile, J. Am. Chem. Soc., 2005, 127, 6528-6529.
- 35 S. Bhosale, A. L. Sisson, P. Talukdar, A. Fürstenberg, N. Banerji, E. Vauthey, G. Bollot, J. Mareda, C. Röger, F. Würthner, N. Sakai and S. Matile, *Science*, 2006, 313, 84-86
- 36 N. Banerji, A. Fürstenberg, S. Bhosale, A. L. Sisson, N. Sakai, S. Matile and E. Vauthey J. Phys. Chem. B, 2008, 112, 8912-8922.
- 37 M. Lista, N. Sakai and S. Matile, Supramol. Chem., 2009, 21, 238-244.
- 835 38 A. L. Sisson, N. Sakai, N. Banerji, A. Fürstenberg, E. Vauthey and S. Matile, *Angew. Chem. Int. Ed.*, 2008, 47, 3727-3729.
 - 39 C.-H. Huang, N. D. McClenaghan, A. Kuhn, G. Bravic, D. M. Bassani, *Tetrahedron*, 2006, 62, 2050–2059.

- 40 J. M. Kerckhoffs, M. G. ten Cate, M. A. Mateos-Timoneda, F. W. van Leeuwen, B. Snellink-Ruel, A. L. Spek, H. Kooijman, M. Crego-Calama and D. N. Reinhoudt, J. Am. Chem. Soc., 2005, 127, 12697-12708.
- 41 J. T. Davis, Angew. Chem. Int. Ed., 2004, 43, 668-698.
- 42 H. Imahori, Y. Mori and Y. Matano, J. Photochem. Photobiol. C: Photochem. Rev., 2003, 4, 51-83.
- 43 S. Fukuzumi, Bull. Chem. Soc. Jpn., 2006, 79, 177-195.
- 44 I. Carmeli, L. Frolov, C. Carmeli and S. Richter, J. Am. Chem. Soc., 2007, 129, 12352-12353.
- 45 T. Takada, C. Lin and T. Majima, Angew. Chem. Int. Ed., 2007, 46, 6681-6683.
 - 46 S. Yasutomi, T. Morita, Y. Imanishi and S. Kimura, *Science*, 2004, 304, 1944-1947.
 - 47 S. Kimura, Org. Biomol. Chem., 2008, 6, 1143-1148.
- D. M. Guldi, I. Zilbermann, G. Anderson, A. Li, D. Balbinot, N. Jux,
 M. Hatzimarinaki, A. Hirsch and Maurizio Prato, *Chem. Commun.*,
 2004, 726-727.
- 49 F. B. Abdelrazzaq, R. C. Kwong and M. E. Thompson, J. Am. Chem. Soc., 2002, 124, 4796-4803.
- M. Morisue, S. Yamatsu, N. Haruta and Y. Kobuke, *Chem. Eur. J.*,
 2005, 11, 5563-5574.
- 51 Y. Rio, M. S. Rodriguez-Morgade and T. Torres, *Org. Biomol. Chem.*, 2008, 6, 1877-1894.
- 52 K. Tahara, T. Fujita, M. Sonoda, M. Shiro and Y. Tobe, *J. Am. Chem. Soc.*, 2008, **130**, 14339-14345.
- 55 53 M. Lopalco, E. N. Koini, J. K. Cho and M. Bradley, Org. Biomol. Chem., 2009, 7, 856-859.
- 54 O. Sadovski, A. A. Beharry, F. Zhang and G. A. Woolley, *Angew. Chem. Int. Ed.*, 2009, 48, 1484-1486.
- R. P. Haugland, The Handbook. A Guide to Fluorescent Probes and Labeling Techniques, 10th Edition, Invitrogen, 2005.
 - 56 R. Koeppe, O. Bossart, G. Calzaferri and N. S. Sariciftci, Sol. Energy Mater. Sol. Cells, 2007, 91, 986–995.
 - 57 R. A. Miller, A. D. Presley and M. B. Francis, J. Am. Chem. Soc., 2007, 129, 3104-3109.
- 5 58 J. Y. Kim, K. Lee, N. E. Coates, D. Moses, T.-Q. Nguyen, M. Dante and A. J. Heeger, *Science*, 2007, 317, 222-225.
- 59 E. A. Weiss, V. J. Porter, R. C. Chiechi, S. M. Geyer, D. C. Bell, M. G. Bawendi and G. M. Whitesides, *J. Am. Chem. Soc.*, 2008, **130**, 83-92
- 880 60 A. Kongkanand, K. Tvrdy, K. Takechi, M. Kuno and P. V. Kamat, J. Am. Chem. Soc., 2008, 130, 4007-4015.
 - S. V. Bhosale, C. H. Jani and S. J. Langford, *Chem. Soc. Rev.*, 2008, 37, 331-342.
- 62 C. Röger and F. Würthner, J. Org. Chem., 2007, 72, 8070-8075.
- 885 63 A. Blaszczyk, M. Fischer, C. von Hänisch, and M. Mayor, *Helv. Chim. Acta*, 2006, 89, 1986-2005.
 - 64 S. Chopin, F. Chaignon, E. Blart and F. Odobel, J. Mater. Chem., 2007, 17, 4139-4146.
- H. Yan, Z. Chen, Y. Zheng, C. Newman, J. R. Quinn, F. Dötz, M.
 Kastler and A. Facchetti, *Nature*, 2009, 457, 679-686.
- 66 F. Würthner, Chem Commun., 2004, 1564-1579.
- 67 R. Bhosale, A. Perez-Velasco, V. Ravikumar, R. S. K. Kishore, O. Kel, A. Gomez-Casado, P. Jonkheijm, J. Huskens, P. Maroni, M. Borkovec, T. Sawada, E. Vauthey, N. Sakai and S. Matile, submitted.



Biodata

Rajesh Bhosale was born in 1977 in Udgir Latur, India. He received his MSc from SRTM, University Nanded, India. In 2005, he moved to the University of Geneva, Switzerland, where he is currently carrying out his PhD. under the supervision of Professor S. Matile. His research is focused on the design, synthesis and evaluation of artificial photosystems.

910 Jiří Míšek received his MSc (2004) and PhD (2008) from the Charles University in Prague and the Institute of Organic Chemistry and Biochemistry in Prague (Czech Republic). During his PhD in the group of Doctor I. Starý he was synthesizing azahelicenes and studying their properties and potential 915 applications. Currently he is a Postdoctoral Roche Fellow in the group of Professor S. Matile in Geneva focusing on various supramolecular approaches to functional photosystems.

Naomi Sakai (middle right) gained her BS from Keio University (1987) and her PhD from Tokushima Bunri University (1994). After a postdoctoral stay in the group of Professor Koji Nakanishi at Columbia University (1994-1996), she focuses on the creation of functional nanoarchitectures for broad applications such as solar cells and biosensors, first in 925 Washington DC (Georgetown University, 1996-1999), then in Geneva (1999-present).

Stefan Matile received his Diploma (1989) and his PhD (1994) from the University of Zurich for research in bioorganic porphyrin chemistry in the group of Wolf Woggon. After a postdoc with Koji Nakanishi at Columbia University, New York, on circular dichroism spectroscopy (1994-1996), he joined the faculty of first Georgetown University, Washington DC (1996-1999) and then the University of Geneva (1999-present). His research interests are at the interface of organic, biological and supramolecular materials chemistry, with current emphasis on multifunctional nanoarchitectures on the rocks and in lipid bilayers, covering topics such as smart photosystems, multianalyte sensing with pores, ion channels and, last but not 940 least, multistep synthesis.